LANGMUIR

pubs.acs.org/Langmuir Article

Frost Delay of a Water-Absorbing Surface with Engineered Wettability via Nonfreezing Water

Bishwash Shrestha, Mohammadamin Ezazi, Vahid Rad, Anjana Maharjan, and Gibum Kwon*

Cite This: *Langmuir* 2022, 38, 5787−5794 Read Online

ACCESS | Metrics & More | Article Recommendations | Supporting Information

ABSTRACT: Frost is common when a solid surface is subjected to a humid and cold environment. It can cause various inconveniences, complications, or fatal accidents. Water-repellent surfaces have demonstrated an antifreezing capability by enabling the water droplets to roll or bounce off before they freeze. However, these surfaces are often limited by their inability to shed the small water condensates, which can eventually grow and freeze. Recently, surfaces that can rapidly absorb and hydrogen bond with these water condensates have demonstrated significant delay in frost formation and growth. This is attributed to a lower freezing temperature of the absorbed water which makes it stay in a nonfreezing state. Herein, we report a surface with preferential wettability of water over oil (i.e., superhydrophilic and oleophobic wettability) that can significantly delay frost formation. The surface is fabricated by copolymerizing poly(ethylene glycol) diacrylate (PEGDA) and perfluorinated acrylate (1*H*,1*H*,2*H*,2*H*-heptadecafluorodecyl acrylate, HDF-acrylate) applied to a silane-grafted glass substrate (HDF-PEGDA). An HDF-PEGDA surface can quickly absorb condensed water which enables it to delay frost formation and growth for up to 20 min at a surface temperature of −35 °C. Also, the surface demonstrates that its frost-resistant capability remains almost unaffected even after being submerged in an oil bath due to its in-air oil repellency. Differential scanning calorimetry (DSC) measurements reveal that the significant quantity of absorbed water in an HDF-PEGDA surface remains in a nonfreezing state with a T_m value as low as −33 °C. A mathematical model that can predict the time at which the surface begins to be covered with frost is developed. Finally, an HDF-PEGDA is layered with a PEGDA copolymerized with sodium acrylate (Na-acrylate) that enables the continuous release of the absorbed water by posing forward osmotic pressure and regeneration of an HDF-PEGDA surface.

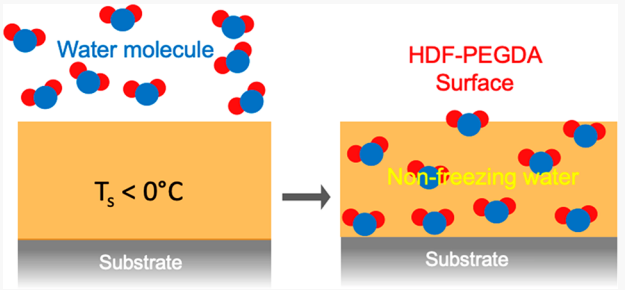

INTRODUCTION

Frigid weather can result in various problems such as power line failure,[1] disturbing aircraft buoyancy,[2] reducing energy efficiency,[3−5] and heat transfer[6,7] and can even lead to fatal accidents[8−11] primarily due to ice or frost formation on a surface. Ice and frost form on a solid surface when the surrounding temperature goes below the freezing point of water (T_m), which decreases the water temperature (T_w) and surface temperature (T_s) below the T_m, leading to freezing. While ice formation needs the presence of bulk liquid water (e.g., rain droplet), frost typically forms when water vapor (e.g., moisture) condenses and freezes on a surface.[12,13] Thus, in most frigid weather conditions, frost is a more ubiquitous phenomenon.[14]

Engineering a surface that can prevent or mitigate frost needs one to consider both thermodynamics and kinetics of the frost formation process.[12,15] A literature survey has revealed that there are two generally accepted frost formation routes.[12,16] A condensation-based one prevails when the dew point (T_d) remains higher than the T_m (i.e., $T_d > T_m$) and $T_s < T_m$, which leads to condensation and freezing, respectively. In contrast, a desublimation-based route takes place when $T_d < T_m$ while $T_s < T_m$. This enables water vapor to directly transition into frost. Given that the T_d is typically higher than T_m at one atmospheric pressure (1 atm), most research efforts have thus far been focused on preventing or mitigating condensation-based frost formation.[17,18]

The simplest method of mitigating frost on a surface is perhaps a direct removal by external triggers, including mechanical abrasion,[19] chemical dissolving,[20,21] and thermal heating.[22,23] While these methodologies are versatile and easy to implement, they often result in physical damage to the surface, environmental pollution, and high energy demand.[24] Porous surfaces[25−27] impregnated by freezing-point-depressant liquid can address the above-mentioned issues. The impregnated liquids provide a lubricating layer that can reduce the adhesion strength of ice to the surfaces. For example, Kim et al.[28] reported a perfluoroalkylether infused surface demonstrating an ice

Received: February 14, 2022
Revised: April 7, 2022
Published: April 21, 2022

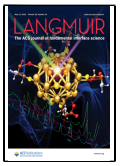

adhesion strength of around 15 kPa which is an order less than that of a conventional surface.

Manipulating the surface wettability is an emerging technology for mitigating or preventing frost formation.[16,29−33] Developing icephobic surfaces that can inhibit frost accretion has been the commonly utilized methodology in this approach.[34−36] Icephobic surfaces generally possess hydrophobic (i.e., water contact angle, $\theta_w > 90°$) or superhydrophobic (i.e., $\theta_w > 150°$ and roll-off angle <5°) wettability which enables low ice adhesion or an antifreezing capability by shedding the condensed water droplets before they freeze.[29,30,37] These surfaces exhibit minimal ice adhesion strength such that the accreted frozen water can be readily removed by its own weight or under the exertion of other forces such as wind shear.[34] Further, these water-repellent surfaces exhibit relatively higher enthalpic energy for the phase transition of water (i.e., liquid water to solid ice), which can lead to a delay in frost formation and growth.[12] While these surfaces can effectively prevent ice formation by repelling water droplets, their performance against condensation freezing is reported to be limited.[38] In a new vein, a hydrophilic (i.e., $\theta_w < 90°$) or superhydrophilic (i.e., $\theta_w \approx 0°$) surface allows the condensed water droplet to rapidly spread and form a thin water film. On these surfaces, the T_m of water can be as low as −40 °C at 1 atm, which has been attributed to hydrogen bonding with hydrophilic moieties [e.g., −OH (hydroxyl) species] on the surface.[31] Taking advantage of this phenomenon, recently, Chen et al.[34] developed an icephobic surface by utilizing a polydimethylsiloxane (PDMS)-poly(ethylene glycol) (PEG) material exhibiting a suppressed freezing temperature for water.

By taking advantage of both hydrophilic (or superhydrophilic) and hydrophobic (or superhydrophobic) surfaces, chemically patterned surfaces (i.e., hydrophilic domains surrounded by hydrophobic background or *vice versa*) have demonstrated that they can delay frost formation and/or growth.[16,32,33] Their performance was governed by the area fraction of hydrophilic and hydrophobic domains, their spatial distribution, and the solid surface free energy (γ_{sv}) of each domain.[16] Nonetheless, condensed water on these surfaces can eventually grow over time and become frost once it forms.[15]

A surface that can quickly absorb and hydrogen bond with the condensed water can be an alternative.[39,40] Lin et al.[40] have demonstrated that a poly(ethylene glycol) (PEG) surface can exhibit a very low T_m of water ($T_m = -40$ °C), which can hamper the transition of liquid water to solid ice. Lee et al.[39] have shown that poly(vinyl alcohol)/poly(acrylic acid) (PVA/PAA) surface-functionalized with PEG can exhibit a frost-resisting capability by rapidly absorbing water and hydrogen bonding with it. Previous reports have shown that the water absorbed by these surfaces remains in a "nonfreezing" state even at a very low T_s. For example, Talik et al.[41] have demonstrated that a hydroxypropyl cellulose surface can retain nonfreezing water at a temperature up to $T_s = -21.6$ °C. Similarly, Rodriguez et al.[42] have also confirmed the presence of such nonfreezing water on a gelatin-chitosan-PVA surface at subzero temperature.

Herein, we report a superhydrophilic and oleophobic [i.e., oil contact angle (θ_o) > 90°] surface by utilizing poly(ethylene glycol) diacrylate (PEGDA) and 1*H*,1*H*,2*H*,2*H*-heptadecafluorodecyl acrylate (HDF-acrylate). An HDF-PEGDA surface shows that it can absorb both bulk liquid water and condensed water that enable it to delay frost formation and growth. Also, it demonstrates that it can remain frost-resisting after being submerged in an oil bath (oil contamination) due to its in-air oil repellency that enables shedding the oils. Differential scanning calorimetry (DSC) results indicate that a significant quantity of absorbed water in an HDF-PEGDA surface remains in a nonfreezing state with a T_m value as low as −33 °C. Also, a mathematical model that can predict the time at which an HDF-PEGDA surface starts to be covered with frost is developed by employing a dropwise condensation model along with the quantity of the nonfreezing water. Finally, HDF-PEGDA is layered with PEGDA copolymerized with sodium acrylate (Na-acrylate) that enables the continuous release of the absorbed water by posing forward osmotic pressure and regeneration of an HDF-PEGDA surface.

EXPERIMENTAL SECTION

Methacryloxypropyl Trimethoxysilane (MPTM)-Silane Grafting on a Substrate. A glass substrate was first thoroughly rinsed using deionized (DI) water to remove any dirt and dust. Then, it was sonicated for 30 min in a solution containing ethanol, acetone, and isopropanol (1:1:1 weight ratio) followed by rinsing with DI water for 5 min. The substrate was then treated with air plasma (400 W) for 5 min to generate hydroxyl species on the surface. Subsequently, the substrate was submerged in an MPTM-silane solution (10 wt % in methanol) for 60 min at room temperature (~22 °C). Then, it was placed on a hot plate at 60 °C for 60 min followed by rinsing with methanol to remove any unreacted silane molecules.

HDF-PEGDA Surface Fabrication. A solution of PEGDA and HDF-acrylate was prepared in water (solute concentration = 200 mg mL^{-1}). Darocur 1173 was added dropwise to the solution (5.0 wt % with respect to the mass of PEGDA and HDF-acrylate). The solution was spin-cast on the MPTM-silane-grafted glass substrate at 1500 rpm for 1 min followed by UV-light irradiation [wavelength (λ) = 365 nm, intensity (I) = 78 mW cm^{-2}] for 30 min. Note that the thickness of an HDF-PEGDA surface can be modulated by varying the concentrations of solutions (e.g., 5, 10, 30, 50, 100, and 200 mg mL^{-1}).

Omniphilic and Omniphobic Surface Fabrication. An omniphilic surface was prepared by oxygen plasma treatment of a clean glass substrate for 5 min. An omniphobic surface was fabricated by grafting 1*H*,1*H*,2*H*,2*H*-perfluorodecyl trichlorosilane onto a clean glass substrate. The substrate was placed in a sealed Teflon jar filled with silane vapor at 130 °C for 1 h. Subsequently, the substrate was rinsed with DI water and ethanol to remove any unreacted silane molecules.

Measurements of the Water Absorption Capacity (w). A surface (2.5 × 2.5 cm^2) was submerged in a DI water bath for 24 h at room temperature (~22.5 °C). The mass of water absorbed by the surface was calculated by subtracting the mass of the dry surface from that of the soaked surface. Note that a thickness of surfaces of ~20 μm was utilized.

Measurements of the Time of Imbibition (ToI). A sessile water droplet (5 μL) was dropped on a surface at ambient conditions (T = 21.3 ± 0.5 °C and RH = 52.5% ± 2.0%). The ToI value was determined when the water droplet was completely imbibed into the surface. To minimize the evaporation effect on the measurements, we conducted the experiment in a controlled enclosed setup keeping the T and RH constant. The test was repeated three times, and a mean with 1σ standard deviation is reported.

Atmospheric Water Condensation. A sample (2.5 × 2.5 cm^2) was first stored in a fridge (−20 °C) for 1 h. Then, the surface was taken out from the fridge and immediately exposed to ambient conditions (T = 22.3 ± 0.7 °C and RH = 50.4% ± 2.2%) under an optical microscope. A movie of the condensation process was recorded utilizing Camtasia software.

Modified Cold−Warm Test. A sample (2.5 × 2.5 cm^2) was placed on a Peltier plate (−35 °C) while it was exposed to ambient conditions (T = 22.3 ± 0.7 °C and RH = 51.4% ± 2.5%). A video camera was placed directly above the sample at a distance of 10 cm to monitor frost formation and growth.

Frost Area Coverage Calculation. A surface area covered by frost as a function of time was calculated by utilizing ImageJ processing of

https://doi.org/10.1021/acs.langmuir.2c00369
Langmuir 2022, 38, 5787−5794

Scheme 1. Synthesis of an HDF-PEGDA Surface on an MPTM-Silane-Grafted Glass Substrate

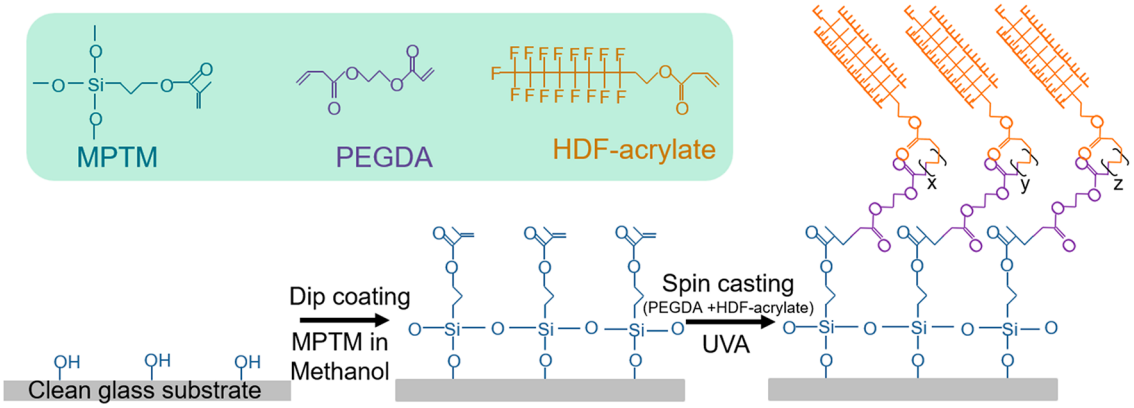

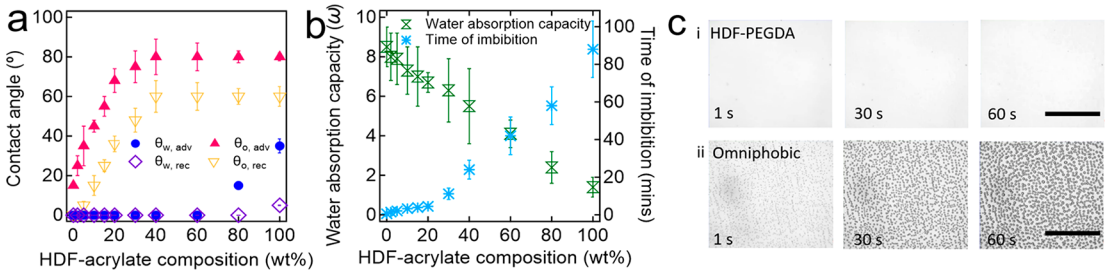

Figure 1. (a) Measured advancing and receding contact angles for oil (*n*-hexadecane) and DI water on an HDF-PEGDA surface prepared with varied HDF-acrylate compositions (wt %). (b) Measured water absorption capacity (w) and time of imbibition (ToI) values of HDF-PEGDA surfaces prepared with varied HDF-acrylate compositions (wt %). (c) Time-lapse images of water vapor condensation on an HDF-PEGDA (i) and omniphobic (ii) surface. Scale bar: 100 μm.

digital images. First, the images were modified to inverted black and white images by ImageJ software. The black pixels represent a frost-covered area. The total number of black pixels divided by that of the entire surface is the area fraction of the frost-covered surface. Each surface was analyzed three times to ensure the accuracy of the measurements.

Differential Scanning Colorimetry for Characterizing Non-freezing Water. An HDF-PEGDA surface (2.5 × 2.5 cm^2) with a known thickness (~20 μm) was utilized. First, the mass of an HDF-PEGDA coating was measured by subtracting the mass of a glass substrate from the mass of a glass substrate coated with HDF-PEGDA. Subsequently, a water droplet with a known mass was placed on a surface until all of the water was absorbed. DSC measurements were conducted by cooling approximately 20 mg of HDF-PEGDA soaked with water from 15 to −60 °C at a cooling rate of −5 °C min^{-1} by utilizing a TA Instruments Q200 differential scanning calorimeter. Note that nitrogen gas at a flow rate of 20 mL min^{-1} was utilized during the measurements.

Measurements of *m* Values. The mass of absorbed water (m) in the HDF-PEGDA surface at varying temperatures was measured by using a weighing balance (Mettler Toledo, ME 103E). The mass of a dry (as-prepared) HDF-PEGDA surface was measured by subtracting the mass of a glass substrate from the mass of a glass substrate coated with HDF-PEGDA. The m value was then calculated by subtracting the dry mass of HDF-PEGDA from the mass of the substrate when 10% of its entire surface area was covered by frost.

Measurements of the Surface Thickness. We utilized optical profilometry (Veeco Wyko NT 1100) to determine the surface thickness. The surface was cut using a scalpel followed by scanning the stepped edge at a scan rate of 300 nm s^{-1}. The measurements were conducted for at least five different places.

Contact Angle Measurements. All contact angles were measured by advancing or receding ~4 μL of liquids onto the surface utilizing a ramé-hart 190-U1 goniometer. Three consecutive measurements were carried out across a surface. The data reported are a mean value with 1σ standard deviation.

HDF-Na-PEGDA Surface Fabrication. First, a solution of PEGDA and Na-acrylate (1:1 weight ratio) was prepared in water (solute concentration = 100 mg mL^{-1}) followed by dropwise addition of Darocur 1173 (5.0 wt % with respect to the mass of PEGDA and Na-acrylate). The solution was spin-cast on the MPTM-grafted glass substrate at 1500 rpm for 1 min. Subsequently, the substrate was irradiated by UV light (λ = 365 nm, I = 78 mW cm^{-2}) for 10 min resulting in partial curing of PEGDA and Na-acrylate (Na-PEGDA). Finally, a solution of HDF-PEGDA (solute concentration = 100 mg mL^{-1}) with Darocur 1173 (5.0 wt %) was spin-cast at 1500 rpm for 1 min followed by UV light irradiation for 30 min.

RESULTS AND DISCUSSION

To fabricate a superhydrophilic and oleophobic surface that can delay the frost initiation, a clean glass substrate was first treated with methacryloxypropyl trimethoxysilane (MPTM-silane). The substrate was dip-coated in an MPTM-silane solution (10.0 wt % in methanol) for 60 min at room temperature ($T \approx$ 22.2 °C). Subsequently, a solution of PEGDA, HDF-acrylate, and Darocur 1173 in deionized (DI) water (total solute concentration = 200 mg mL^{-1}) was spin-cast on the MPTM-silane-grafted substrate (Scheme 1, see the Experimental Section). Then, the substrate was irradiated by ultraviolet (UV) light [wavelength = 365 nm, intensity (I) = 78 mW cm^{-2}] for 30 min. This results in a cross-linked coating of the PEGDA and HDF-acrylate (thickness = 20.1 ± 0.2 μm) grafted onto the MPTM layer (HDF-PEGDA surface; Section S1 in the Supporting Information).

We measured the advancing (θ_{adv}) and receding (θ_{rec}) contact angles for an oil (*n*-hexadecane, γ_{lv} = 27.5 mN m^{-1}) and DI water (γ_{lv} = 72.1 mN m^{-1}) on the HDF-PEGDA surfaces prepared

https://doi.org/10.1021/acs.langmuir.2c00369
Langmuir 2022, 38, 5787−5794

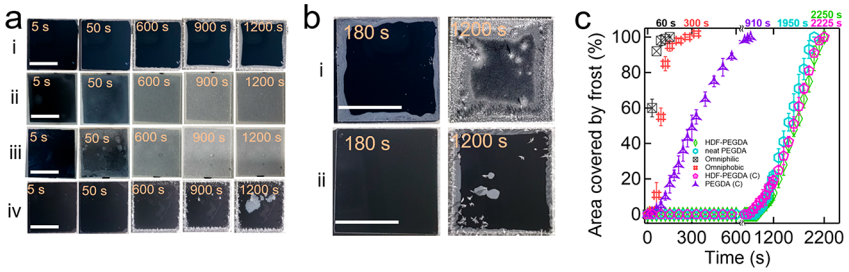

Figure 2. (a) Time-lapse images of (i) HDF-PEGDA, (ii) omniphilic, (iii) omniphobic, and (iv) neat PEGDA surfaces placed on a Peltier plate at T = −35 °C exposed to ambient conditions (T = 22.3 ± 0.7 °C and RH = 51.4% ± 2.5%). Scale bar = 15 mm. (b) Time-lapse images of oil-contaminated neat PEGDA and HDF-PEGDA surfaces placed on a Peltier plate at T = −35 °C exposed to ambient conditions (T = 22.1 ± 0.3 °C and RH = 53.5% ± 1.7%). (c) Time-dependent evolution of the surface area fraction (%) covered by the frost of HDF-PEGDA, neat PEGDA, omniphilic, and omniphobic surfaces. The data of oil-contaminated HDF-PEGDA (C) and neat PEGDA (C) surfaces are also shown.

with varied HDF-acrylate compositions. The results show that a surface with a higher HDF-acrylate composition exhibits a higher oil contact angle (Figure 1a). The values of $\theta_{adv,oil}$ and $\theta_{rec,oil}$ become nearly constant ($\theta_{adv,oil}$ = 81° ± 5° and $\theta_{rec,oil}$ = 60° ± 4°, respectively) on the HDF-PEGDA surfaces with HDF-acrylate composition greater than 20 wt %. This can be attributed to the fluorinated moieties (e.g., $-CF_2$ or $-CF_3$) that covered nearly the entire surface.[43−45] Note that the contact angles for water ($\theta_{adv,water}$ and $\theta_{rec,water}$) remain zero on the HDF-PEGDA surfaces fabricated with HDF-acrylate compositions below 80 wt %. Such a preferential wettability for water over oil (i.e., superhydrophilic and oleophobic) has been attributed to surface reconfiguration upon contacting water.[43,46]

Preventing frost formation and growth requires prompt removal of the water condensates from the surface before freezing. PEGDA is a hydrogel that can spontaneously absorb water in ambient conditions.[47] We measured the HDF-PEGDA surface's water absorption capacity (ω) by

$$\omega = (W_t - W_0)/W_0 \quad (1)$$

where W_0 and W_t are the mass of a dry HDF-PEGDA surface and that after absorbing water for the duration t, respectively (Experimental Section). The results show that an HDF-PEGDA surface with a higher HDF-acrylate composition exhibits a lower ω value (Figure 1b). This is because a neat HDF-acrylate (i.e., HDF-acrylate composition = 100 wt %) absorbs a significantly lower amount of water (ω = 1.7 ± 0.1) compared with a neat PEGDA (i.e., HDF-acrylate composition = 0) which exhibits ω = 8.3 ± 1.1.

We also measured the time required for an HDF-PEGDA surface to absorb a sessile water droplet (~5 μL) placed on it (i.e., time of imbibition, ToI, Experimental Section). An HDF-PEGDA surface with a higher HDF-acrylate composition shows a higher ToI value (Figure 1b). Similar to the ω, the ToI is also affected by the amount of PEGDA in the surface (i.e., the composition of HDF-acrylate). This is because the water imbibition process is driven by PEGDA−water hydrogen bonding and the resulting surface reconfiguration.[43,47] Thus, a lower amount of PEGDA in the surface can lead to a longer time required for the progress and completion of surface reconfiguration. The same experiments of water absorption and imbibition were conducted by using HDF-PEGDA surfaces prepared with varied Darocur 1173 concentrations (Section S2). Note that the evaporation of a probing water droplet during the imbibition tests was negligible (Section S3). Based on the results of the contact angle measurements, water absorption, and imbibition tests, we utilized an HDF-PEGDA surface with 20 wt % HDF-acrylate compositions throughout this report.

We tested atmospheric water condensation on the HDF-PEGDA surface (Experimental Section). First, the surface was stored in a fridge at −20 °C for 1 h. Then, it was taken out from the fridge and immediately exposed to ambient conditions [T = 22.3 ± 0.7 °C and relative humidity (RH) = 50.4% ± 2.2%]. The time-lapse optical microscopy images of the HDF-PEGDA surface show no visible water condensates on it (Figure 1c,i). In contrast, an omniphobic (i.e., hydrophobic and oleophobic) surface (Experimental Section) is covered by water condensates instantaneously after being exposed to ambient conditions (Figure 1c,ii). Such difference can be attributed to the fact that the HDF-PEGDA surface can rapidly absorb molecular water from the environment before it can change the state of matter from the gas phase to the liquid phase,[39,48] whereas it undergoes a phase change to a water droplet on the omniphobic surface without absorption. Note that the ToI for a sessile water droplet was measured as ToI = 5.5 ± 0.5 min (see also Figure 1b).

Encouraged by this result, we conducted a modified cold−warm test[48] to assess the HDF-PEGDA surface's capability of suppressing frost formation and growth (Experimental Section). The substrate was placed on a thermoelectric cooler (Peltier plate) with a temperature of −35 °C while exposed to the ambient air (t = 0, T = 22.3 ± 0.7 °C and RH = 51.4% ± 2.5%). We found that the frost starts to appear (i.e., frost initiation) on the HDF-PEGDA surface at t = 1195 ± 35 s (Figure 2a,i). Here, the time of frost initiation (t_{frost}) is determined when frost covers greater than 10% of the surface area (Experimental Section). For comparison, we conducted the same experiment by using an omniphilic [i.e., hydrophilic and oleophilic (θ_o < 90°)] surface and an omniphobic surface (Experimental Section). The frost initiation was observed at t_{frost} = 4 ± 3 s on an omniphilic surface (Figure 2a,ii) while it was observed at t_{frost} = 45 ± 6 s on an omniphobic surface (Figure 2a,iii). A movie demonstrating frost initiation on an omniphilic, omniphobic, and HDF-PEGDA surface is included in the Supporting Information (Movie S1). Note that both omniphilic and omniphobic surfaces exhibit negligible water absorption (Section S4). A slightly longer delay in the frost initiation of an omniphobic surface can be attributed to its higher water contact angles ($\theta_{adv,water}$ = 95° ± 3° and $\theta_{rec,water}$ = 63° ± 2°) compared to those on an omniphilic surface ($\theta_{adv,water}$ = 7° ± 3° and $\theta_{rec,water}$ = 0°) that can provide a lower interfacial area for heat conduction between the water droplet and the surface.[49] While a neat PEGDA surface also exhibits hydrophilic wettability ($\theta_{adv,water}$ = 5° ± 5° and $\theta_{rec,water}$ = 0°, see also Figure 1a), unlike an omniphilic surface, it demonstrates the

https://doi.org/10.1021/acs.langmuir.2c00369
Langmuir 2022, 38, 5787−5794

frost initiation at t_{frost} = 1153 ± 45 s (Figure 2a,iv) which is comparable to that observed on an HDF-PEGDA. This is because a neat PEGDA can also absorb the water condensates.

While as-prepared neat PEGDA and HDF-PEGDA surfaces showed a similar delay in the frost initiation, it is postulated that their performances can differ when they are subjected to organic contaminants (e.g., oils). To verify this, both surfaces were submerged in an oil bath (*n*-heptane, γ_{lv} = 20.1 mN m^{-1}) for 10 min. They were withdrawn vertically at a constant speed of 5 mm s^{-1}. Subsequently, both surfaces were placed on a Peltier plate (T = −35 °C) in ambient conditions (T = 22.1 ± 0.3 °C and RH = 53.5% ± 1.7%). The frost initiation was observed at t_{frost} = 175 ± 20 s on a neat PEGDA surface (Figure 2b,i). This can be attributed to the oil which can remain on the surface and serve as the frost nucleation sites (Movie S2). In contrast, the HDF-PEGDA surface exhibited frost initiation at t_{frost} = 1141 ± 30 s (Figure 2b,ii), which is comparable to that observed on an as-prepared surface. This is because the HDF-PEGDA surface enables the oil to slide off during the withdrawing process due to its low contact angle hysteresis (Δ, $\Delta = \theta_{adv,oil} - \theta_{rec,oil}$) for oil (see also Figure 1a). Also, water can displace the oil and be absorbed on the HDF-PEGDA surface,[43,44,50] which contributes to maintaining its frost delaying capability after surface contamination. For comparison, we conducted the same experiments by using an omniphilic and an omniphobic surface. The frost initiation was observed at t_{frost} = 30 ± 12 s and at t_{frost} = 55 ± 10 s on an omniphilic surface and an omniphobic surface, respectively (Section S5). The effect of the amount of remnant oil on the frost initiation behaviors is summarized in Section S6. The time-dependent evolution of the surface area covered by frost was quantitatively and digitally analyzed by using ImageJ (Figure 2c, Experimental Section). The results show that as-prepared HDF-PEGDA and neat PEGDA surfaces were completely covered by frost at t_c = 2250 ± 10 s and t_c = 1950 ± 25 s, respectively, whereas omniphilic and omniphobic surfaces showed 100% frost coverage at t_c = 60 ± 10 s and t_c = 300 ± 30 s, respectively. Note that an oil-contaminated neat PEGDA surface became completely covered by frost at t_c = 910 ± 50 s while a contaminated HDF-PEGDA surface showed a nearly unchanged frost evolution (t_c = 2225 ± 30 s).

A significant delay in the frost initiation of the HDF-PEGDA surface compared with an omniphobic or omniphilic surface can be attributed to its capability to retain the absorbed water in a nonfreezing state.[51] Previous reports have demonstrated that the absorbed water molecules can exhibit a nonrandomized orientation when they form a hydrogen bond with a surface with a strength greater than their intermolecular (i.e., water−water) hydrogen bond strength.[40,51] These water molecules with a nonrandomized orientation remain unfrozen even when the temperature (T_w) is significantly lower than the T_m (Figure 3a,i).[51] In contrast, when water molecules do not form hydrogen bonds with a surface, they can transition to frost by forming a hexagonal structure when T_w becomes lower than the T_m (Figure 3a,ii).

Differential scanning calorimetry (DSC) was conducted to measure the nonfreezing water absorbed in the HDF-PEGDA surface (Experimental Section). The DSC results show that an HDF-PEGDA surface with absorbed water exhibits an endothermic peak while a dry HDF-PEGDA surface does not demonstrate any noticeable peaks (Figure 3b). For example, an HDF-PEGDA surface with 23 wt % absorbed water (i.e., 23 wt % with respect to HDF-PEGDA mass, 10.0 mg) shows a peak at T ≈ −33 °C. This implies that an HDF-PEGDA surface can retain

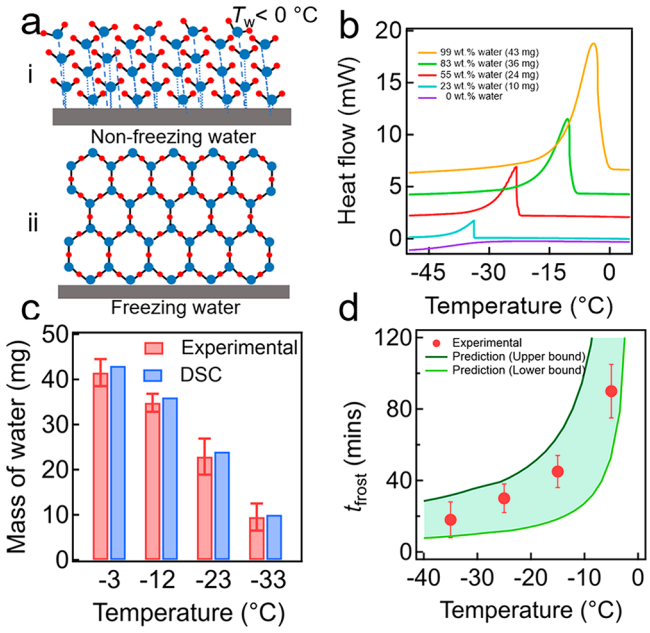

Figure 3. (a) Schematic illustrating the water molecules on a surface when they are in a nonfreezing state (top) or a freezing-state (bottom). The dotted line represents the interaction between the hydrophilic moieties [e.g., −OH (hydroxyl) species] of the surface and water molecules also known as hydrogen bond strength. (b) Differential scanning calorimetry (DSC) data of HDF-PEGDA soaked with varied DI water quantities. (c) Measured mass of water (m) of an HDF-PEGDA surface at varied temperatures until frost initiation begins on the surface. For comparison, the mass of nonfreezing water determined by DSC analyses is also shown. (d) Plot showing the measured t_{frost} values and the predicted values using eq 3.

10.0 mg of the absorbed water in a nonfreezing state up to ∼−33 °C. To verify this, we measured the mass of the absorbed water condensate (m) in HDF-PEGDA surfaces at varied temperatures (−3, −12, −23, and −33 °C, Figure 3c). Note that the m value was measured until the frost initiation was observed. The results show that an HDF-PEGDA surface absorbed 41.5 ± 3.0, 34.8 ± 2.1, 22.9 ± 4.1, and 9.5 ± 3.2 mg at T = −3, −12, −23, and −33 °C, respectively. These values are in reasonable agreement with the DSC data, indicating that frost initiation takes place on an HDF-PEGDA surface when the total mass of the absorbed water (m) becomes equal or greater than the nonfreezing water. The measured m values in HDF-PEGDA surfaces with varied thickness values are included in Section S7.

A mathematical relation that can determine the t_{frost} value on an HDF-PEGDA surface was proposed. Based on a simple dropwise condensation model, the mass increase rate ($\dot{M}$) of the water condensates on a surface is given as[52]

$$\dot{M} = NA\rho\frac{\pi}{3}(2 - 3\cos\theta_w + \cos^3\theta_w)\Delta(r^3) \quad (2)$$

where N is the nucleation rate per unit area, A is the area of the substrate, ρ is the density of water, θ_w is the contact angle of water on the surface, and r is the radius of a condensate droplet. By dividing the experimentally measured m by $\dot{M}$ (eq 2), we obtain a relation of t_{frost} as

$$t_{frost} = m/\dot{M} = \frac{m}{NA\rho\frac{\pi}{3}(2 - \cos\theta_w + \cos^3\theta_w)\Delta(r^3)} \quad (3)$$

Figure 3d shows the values of t_{frost} predicted by using eq 3. Here, we utilized the values reported in the literature (i.e., $N = 3 \times 10^{16}$

https://doi.org/10.1021/acs.langmuir.2c00369
Langmuir 2022, 38, 5787−5794

to 5×10^{15} cm^{-2} s^{-1},[53−55] $A = 6.25$ cm^2, $\rho = 1.0$ g cm^{-3}, $\theta_w = 0$, $\Delta(r^3) = 1.5 \times 10^{-6}$ cm^3[53,54]). For comparison, the experimentally measured values shown in Figure 2c are also shown in this plot. Both the predicted and experimentally measured values match reasonably well.

It is clear from eq 3 that the value of t_{frost} for an HDF-PEGDA surface at given conditions (i.e., N, R, and θ are constant) linearly increases with an increase of the m value. To achieve this, we engineered our HDF-PEGDA surface to regenerate itself by continuously draining the absorbed water to a sink layer. This will enable the surface to continuously absorb water even beyond the m value. We utilized a copolymer of sodium acrylate (Na-acrylate) and PEGDA as a sink layer (Na-PEGDA) (Experimental Section). HDF-PEGDA (thickness = 10.1 ± 0.1 μm) was then deposited on top of the Na-PEGDA layer (thickness = 10.0 ± 0.2 μm). A surface consisting of HDF-PEGDA and Na-PEGDA (i.e., HDF-Na-PEGDA) enables drawing the absorbed water molecules from the HDF-PEGDA layer to the Na-PEGDA layer due to a forward osmotic pressure (Figure 4a). As a result, it is anticipated that the topmost HDF-

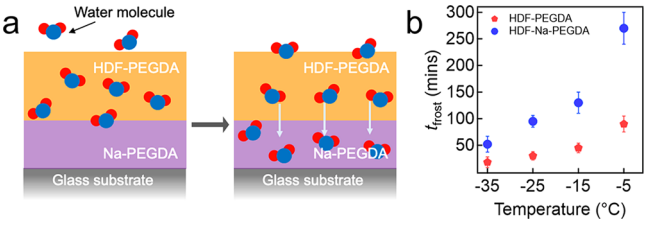

Figure 4. (a) Schematic illustrating the proposed forward osmotic pressure-driven regeneration of an HDF-PEGDA surface layered with Na-PEGDA. (b) Measured t_{frost} values of an HDF-Na-PEGDA surface. For comparison, the t_{frost} values of an HDF-PEGDA surface are also shown.

PEGDA surface can exhibit a higher t_{frost} value. Using this HDF-Na-PEGDA surface, we conducted a modified cold−warm test using a Peltier plate with a temperature of −35 °C while exposed to ambient conditions ($T = 23.1 \pm 1.3$ °C and RH = 52.0% ± 0.2%). The measured t_{frost} value was $t_{frost} = 52.4 \pm 12$ min which is approximately 2.7 times higher than that observed in the HDF-PEGDA surface (Figure 4b). The measured t_{frost} values of the HDF-Na-PEGDA surface at varied temperatures are also significantly higher compared to those observed in the HDF-PEGDA surface (Figure 4b).

CONCLUSION

In conclusion, we fabricated an HDF-PEGDA surface with superhydrophilic and oleophobic wettability. The surface demonstrated that it could absorb both sessile liquid water droplets and molecular water vapor that enable it to delay frost formation and growth. Unlike a neat PEGDA surface, an HDF-PEGDA surface showed that it could maintain its frost-resistant capability after being submerged in an oil bath due to its in-air oleophobic wettability, which enables shedding the oils. DSC data indicate that the absorbed water in the HDF-PEGDA surface remains in a nonfreezing state with a T_m value as low as −33 °C. We developed a mathematical model that can predict the t_{frost} on an HDF-PEGDA surface. Finally, we demonstrated that a surface consisting of HDF-PEGDA layered with Na-PEGDA can continuously release the absorbed water via forward osmotic pressure resulting in the regeneration of an HDF-PEGDA surface.

ASSOCIATED CONTENT

Supporting Information

The Supporting Information is available free of charge at https://pubs.acs.org/doi/10.1021/acs.langmuir.2c00369.

Modulating the thickness of HDF-PEGDA; effect of the concentration of Darocur 1173 on the time of imbibition (ToI); water evaporation during the imbibition tests; negligible water absorption capacity of omniphilic and omniphobic surfaces; frost initiation on an oil contaminated omniphilic and omniphobic surface; effect of oil remnant on the frost initiation; and measurements of the absorbed water mass (m) on HDF-PEGDA surfaces with varied thicknesses (PDF)

Movie S1: frost initiation on an omniphilic, omniphobic, and HDF-PEGDA surface (MP4)

Movie S2: frost initiation as a result of oil contamination (MP4)

AUTHOR INFORMATION

Corresponding Author

Gibum Kwon − *Department of Mechanical Engineering, University of Kansas, Lawrence, Kansas 66045, United States;* orcid.org/0000-0002-7192-1910; Email: gbkwon@ku.edu

Authors

Bishwash Shrestha − *Department of Mechanical Engineering, University of Kansas, Lawrence, Kansas 66045, United States;* orcid.org/0000-0003-0045-8890

Mohammadamin Ezazi − *Department of Mechanical Engineering, University of Kansas, Lawrence, Kansas 66045, United States;* orcid.org/0000-0003-2284-9809

Vahid Rad − *Department of Mechanical Engineering, University of Kansas, Lawrence, Kansas 66045, United States;* orcid.org/0000-0002-6702-2461

Anjana Maharjan − *Department of Mechanical Engineering, University of Kansas, Lawrence, Kansas 66045, United States*

Complete contact information is available at: https://pubs.acs.org/10.1021/acs.langmuir.2c00369

Author Contributions

B.S. and M.E. performed the experiments, analyzed data, and wrote the manuscript. V.R. and A.M. performed experiments. G.K. conceived the project, designed the experiments, and wrote the manuscript.

Notes

The authors declare no competing financial interest.

ACKNOWLEDGMENTS

This research was supported by the National Science Foundation [award CBET-1944314], NASA Kansas EPSCoR [award R52123-20-02314], University of Kansas (KU) Office of Research—General Research Funds, and Research GO. We also thank Dr. J. Kang at the University of Illinois and Dr. Ahn at the University of Texas for the use of facilities.

REFERENCES

(1) Busby, J. W.; Baker, K.; Bazilian, M. D.; Gilbert, A. Q.; Grubert, E.; Rai, V.; Rhodes, J. D.; Shidore, S.; Smith, C. A.; Webber, M. E. Cascading risks: Understanding the 2021 winter blackout in Texas. *Energy Res. Soc. Sci.* **2021**, *77*, 102106.

(2) Gent, R. W.; Dart, N. P.; Cansdale, J. T. Aircraft icing. *P Philos. Trans. R. Soc. London. Series A: Math., Phys. and Eng. Sci.* **2000**, *358* (1776), 2873−2911.
(3) Carriveau, R.; Edrisy, A.; Cadieux, P.; Mailloux, R. Ice adhesion issues in renewable energy infrastructure. *J. Adhes. Sci. Technol.* **2012**, *26* (4−5), 447−461.
(4) Cucchiella, F.; D'Adamo, I. Estimation of the energetic and environmental impacts of a roof-mounted building-integrated photovoltaic systems. *Renew. Sustainable Energy Rev.* **2012**, *16* (7), 5245−5259.
(5) Jelle, B. P. The challenge of removing snow downfall on photovoltaic solar cell roofs in order to maximize solar energy efficiency—Research opportunities for the future. *Energy Build.* **2013**, *67*, 334−351.
(6) Machielsen, C.; Kerschbaumer, H. Influence of frost formation and defrosting on the performance of air coolers: standards and dimensionless coefficients for the system designer. *Int. J. Refri.* **1989**, *12* (5), 283−290.
(7) Zhang, P.; Lv, F. A review of the recent advances in superhydrophobic surfaces and the emerging energy-related applications. *Energy* **2015**, *82*, 1068−1087.
(8) Kraj, A. G.; Bibeau, E. L. Phases of icing on wind turbine blades characterized by ice accumulation. *Renew. Energy* **2010**, *35* (5), 966−972.
(9) Menini, R.; Farzaneh, M. Elaboration of Al2O3/PTFE icephobic coatings for protecting aluminum surfaces. *Surf. Coat. Technol.* **2009**, *203* (14), 1941−1946.
(10) Lee, H.; Shin, J.; Ha, S.; Choi, B.; Lee, J. Frost formation on a plate with different surface hydrophilicity. *Int. J. Heat Mass Transfer* **2004**, *47* (22), 4881−4893.
(11) Smead, R. G. ERCOT—the eyes of Texas (and the World) are upon you: what can be done to avoid a February 2021 repeat. *Climate and Energy* **2021**, *37* (10), 14−18.
(12) Nath, S.; Boreyko, J. B. On localized vapor pressure gradients governing condensation and frost phenomena. *Langmuir* **2016**, *32* (33), 8350−8365.
(13) Hayashi, Y.; Aoki, A.; Adachi, S.; Hori, K. Study of frost properties correlating with frost formation types. *J. Heat Transfer* **1977**, *99* (2), 239−245.
(14) Jones, B.; Parker, J. Frost formation with varying environmental parameters. *J. Heat Transfer* **1975**, *97* (2), 255−259.
(15) Nath, S.; Ahmadi, S. F.; Boreyko, J. B. A review of condensation frosting. *Nanoscale Microscale Thermophys. Eng.* **2017**, *21* (2), 81−101.
(16) Boreyko, J. B.; Hansen, R. R.; Murphy, K. R.; Nath, S.; Retterer, S. T.; Collier, C. P. Controlling condensation and frost growth with chemical micropatterns. *Sci. Rep.* **2016**, *6* (1), 1−15.
(17) Esmeryan, K. D.; Castano, C. E.; Mohammadi, R.; Lazarov, Y.; Radeva, E. I. Delayed condensation and frost formation on superhydrophobic carbon soot coatings by controlling the presence of hydrophilic active sites. *J. Phys. D: Appl. Phys.* **2018**, *51* (5), 055302.
(18) Wang, F.; Liang, C.; Zhang, X. Research of anti-frosting technology in refrigeration and air conditioning fields: A review. *Renew. Sustainable Energy Rev.* **2018**, *81*, 707−722.
(19) Xu, O.; Han, S.; Liu, Y.; Li, C. Experimental investigation surface abrasion resistance and surface frost resistance of concrete pavement incorporating fly ash and slag. *Int. J. Pavement Eng.* **2021**, *22* (14), 1858−1866.
(20) Slate, F. In *Use of Calcium Chloride in Subgrade Soils for Frost Prevention*, Highway Research Board Proceedings, 1943.
(21) Chatterjee, R.; Beysens, D.; Anand, S. Delaying ice and frost formation using phase-switching liquids. *Adv. Mater.* **2019**, *31* (17), 1807812.
(22) Liu, Z.; Li, A.; Wang, Q.; Chi, Y.; Zhang, L. Experimental study on a new type of thermal storage defrosting system for frost-free household refrigerators. *Appl. Therm. Eng.* **2017**, *118*, 256−265.
(23) Wang, Z.; Song, M.; Wang, F.; Ma, Z.; Lin, Q. Experimental investigation and seasonal performance assessment of a frost-free ASHP system with radiant floor heating. *Energy Build.* **2018**, *179*, 200−212.
(24) Liao, Y.; Liu, J.; Chen, S. Research progress of damage mechanism of frost heave and anti-frost technique of concrete canal. *Rock Soil Mech.* **2008**, *29* (S1), 211−214.
(25) Sun, X.; Damle, V. G.; Liu, S.; Rykaczewski, K. Bioinspired stimuli-responsive and antifreeze-secreting anti-icing coatings. *Adv. Mater. Interfaces* **2015**, *2* (5), 1400479.
(26) Ozbay, S.; Yuceel, C.; Erbil, H. Y. Improved icephobic properties on surfaces with a hydrophilic lubricating liquid. *ACS Appl. Mater. Interfaces* **2015**, *7* (39), 22067−22077.
(27) Wilson, P. W.; Lu, W.; Xu, H.; Kim, P.; Kreder, M. J.; Alvarenga, J.; Aizenberg, J. Inhibition of ice nucleation by slippery liquid-infused porous surfaces (SLIPS). *Phys. Chem. Chem. Phys.* **2013**, *15* (2), 581−585.
(28) Kim, P.; Wong, T.-S.; Alvarenga, J.; Kreder, M. J.; Adorno-Martinez, W. E.; Aizenberg, J. Liquid-infused nanostructured surfaces with extreme anti-ice and anti-frost performance. *ACS Nano* **2012**, *6* (8), 6569−6577.
(29) He, M.; Wang, J.; Li, H.; Jin, X.; Wang, J.; Liu, B.; Song, Y. Superhydrophobic film retards frost formation. *Soft Matter* **2010**, *6* (11), 2396−2399.
(30) Boreyko, J. B.; Collier, C. P. Delayed frost growth on jumping-drop superhydrophobic surfaces. *ACS Nano* **2013**, *7* (2), 1618−1627.
(31) Jung, S.; Dorrestijn, M.; Raps, D.; Das, A.; Megaridis, C. M.; Poulikakos, D. Are superhydrophobic surfaces best for icephobicity? *Langmuir* **2011**, *27* (6), 3059−3066.
(32) Yao, Y.; Zhao, T. Y.; Machado, C.; Feldman, E.; Patankar, N. A.; Park, K.-C. Frost-free zone on macrotextured surfaces. *Proc. Natl. Acad. Sci. U.S.A.* **2020**, *117* (12), 6323−6329.
(33) Liu, X.; Chen, H.; Zhao, Z.; Zhu, Y.; Wang, Z.; Chen, J.; Zhang, D. Tunable self-jumping of melting frost on macro-patterned anisotropic superhydrophobic surfaces. *Surf. Coat. Technol.* **2021**, *409*, 126858.
(34) Chen, D.; Gelenter, M. D.; Hong, M.; Cohen, R. E.; McKinley, G. H. Icephobic surfaces induced by interfacial nonfrozen water. *ACS Appl. Mater. Interfaces* **2017**, *9* (4), 4202−4214.
(35) Emelyanenko, K. A.; Emelyanenko, A. M.; Boinovich, L. B. Water and ice adhesion to solid surfaces: Common and specific, the impact of temperature and surface wettability. *Coatings* **2020**, *10* (7), 648.
(36) Irajizad, P.; Nazifi, S.; Ghasemi, H. Icephobic surfaces: Definition and figures of merit. *Adv. Colloid Interface Sci.* **2019**, *269*, 203−218.
(37) Li, X.; Wang, G.; Moita, A. S.; Zhang, C.; Wang, S.; Liu, Y. Fabrication of bio-inspired non-fluorinated superhydrophobic surfaces with anti-icing property and its wettability transformation analysis. *Appl. Surf. Sci.* **2020**, *505*, 144386.
(38) Jamil, M. I.; Ali, A.; Haq, F.; Zhang, Q.; Zhan, X.; Chen, F. Icephobic strategies and materials with superwettability: design principles and mechanism. *Langmuir* **2018**, *34* (50), 15425−15444.
(39) Lee, H.; Alcaraz, M. L.; Rubner, M. F.; Cohen, R. E. Zwitter-wettability and antifogging coatings with frost-resisting capabilities. *ACS Nano* **2013**, *7* (3), 2172−2185.
(40) Lin, C.; Gitsov, I. Synthesis and physical properties of reactive amphiphilic hydrogels based on poly (p-chloromethylstyrene) and poly (ethylene glycol): Effects of composition and molecular architecture. *Macromolecules* **2010**, *43* (7), 3256−3267.
(41) Talik, P.; Hubicka, U. The DSC approach to study non-freezing water contents of hydrated hydroxypropylcellulose (HPC). *J. Therm. Anal. Calorim.* **2018**, *132* (1), 445−451.
(42) Rodríguez-Rodríguez, R.; García-Carvajal, Z.; Jiménez-Palomar, I.; Jiménez-Avalos, J.; Espinosa-Andrews, H. Development of gelatin/chitosan/PVA hydrogels: Thermal stability, water state, viscoelasticity, and cytotoxicity assays. *J. Appl. Polym. Sci.* **2019**, *136* (10), 47149.
(43) Kota, A. K.; Kwon, G.; Choi, W.; Mabry, J. M.; Tuteja, A. Hygro-responsive membranes for effective oil-water separation. *Nat. Commun.* **2012**, *3* (1), 1−8.
(44) Shrestha, B.; Ezazi, M.; Kwon, G. Engineered Nanoparticles with Decoupled Photocatalysis and Wettability for Membrane-Based Desalination and Separation of Oil-Saline Water Mixtures. *Nanomaterials* **2021**, *11* (6), 1397.

https://doi.org/10.1021/acs.langmuir.2c00369
Langmuir 2022, 38, 5787−5794

(45) Shrestha, B.; Ezazi, M.; Kwon, G. Delamination-Free In-Air and Underwater Oil-Repellent Filters for Oil-Water Separation: Gravity-Driven and Cross-Flow Operations. *Energies* **2021**, *14* (21), 7429.
(46) Kwon, G.; Post, E.; Tuteja, A. Membranes with selective wettability for the separation of oil-water mixtures. *MRS Commun.* **2015**, *5* (3), 475−494.
(47) Erol, O.; Pantula, A.; Liu, W.; Gracias, D. H. Transformer hydrogels: a review. *Adv. Mater. Technol.* **2019**, *4* (4), 1900043.
(48) Bai, S.; Li, X.; Zhang, R.; Li, C.; Zhu, K.; Sun, P.; Zhao, Y.; Ren, L.; Yuan, X. Enhancing antifogging/frost-resisting performances of amphiphilic coatings via cationic, zwitterionic or anionic polyelectrolytes. *Chem. Eng. J.* **2019**, *357*, 667−677.
(49) Liu, Z.; Gou, Y.; Wang, J.; Cheng, S. Frost formation on a super-hydrophobic surface under natural convection conditions. *Int. J. Heat Mass Transfer* **2008**, *51* (25−26), 5975−5982.
(50) Pan, Y.; Liu, L.; Zhang, Z.; Huang, S.; Hao, Z.; Zhao, X. Surfaces with controllable super-wettability and applications for smart oil-water separation. *Chem. Eng. J.* **2019**, *378*, 122178.
(51) Wolfe, J.; Bryant, G.; Koster, K. L. What is' unfreezable water', how unfreezable is it and how much is there? *CryoLetters* **2002**, *23* (3), 157−166.
(52) Sikarwar, B. S.; Khandekar, S.; Muralidhar, K. Mathematical modelling of dropwise condensation on textured surfaces. *Sadhana* **2013**, *38* (6), 1135−1171.
(53) Weisensee, P. B.; Wang, Y.; Qian, H.; Schultz, D.; King, W. P.; Miljkovic, N. Condensate droplet size distribution on lubricant-infused surfaces. *Int. J. Heat Mass Transfer* **2017**, *109*, 187−199.
(54) Graham, C.; Griffith, P. Drop size distributions and heat transfer in dropwise condensation. *Int. J. Heat Mass Transfer* **1973**, *16* (2), 337−346.
(55) Rose, J. Further aspects of dropwise condensation theory. *Int. J. Heat Mass Transfer* **1976**, *19* (12), 1363−1370.

https://doi.org/10.1021/acs.langmuir.2c00369
Langmuir 2022, 38, 5787−5794